ACS Sustainable Chemistry & Engineering

Research Article

pubs.acs.org/journal/ascecg

Effect of Structure on the Electrochemical Performance of Nitrogen- and Oxygen-Containing Carbon Micro/Nanospheres Prepared from Lignin-Based Composites

Zhi-Wei He, Jun Yang, Qiu-Feng Lü,* and Qilang Lin

College of Materials Science and Engineering, Fuzhou University, 2 Xueyuan Road, Fuzhou 350116, P. R. China

Supporting Information

ABSTRACT: Nitrogen- and oxygen-containing carbon micro/nanospheres (C_{PAN} and C_{PNA}) were prepared by direct pyrolysis of lignosulfonate/polyaniline and lignosulfonate/poly(*N*-ethylaniline) composite spheres at the temperature of 700 °C. The two type lignin-based composite spheres were prepared by an in situ polymerization of aniline and *N*-ethylaniline in the presence of lignosulfonate, respectively. The carbon spheres were investigated by thermal gravimetric analysis, scanning electron microscopy, transmission electron microscopy, Fourier transform infrared spectroscopy, X-ray diffraction, and X-ray photoelectron spectroscopy and were used as anodes for lithium ion batteries. The two carbon spheres showed different electrochemical performances due to their different surface functional groups and structures. The C_{PAN} carbon nanospheres had better electrochemical performance as anodes for lithium ion batteries than that of C_{PNA} carbon microspheres. The first charge capacity and discharge capacity of the C_{PAN} nanospheres at a current density of 60, 100, and 200 mA g^{-1} exhibited a discharge capacity of 1450, 1094, and 770 mAh g^{-1}, respectively, and a charge capacity of 707, 698, and 446 mAh g^{-1}, respectively. Furthermore, it still owned a high discharge capacity at a current density of 60, 100, and 200 mA g^{-1} of 526, 431, and 338 mAh g^{-1}, respectively, after 20 cycles.

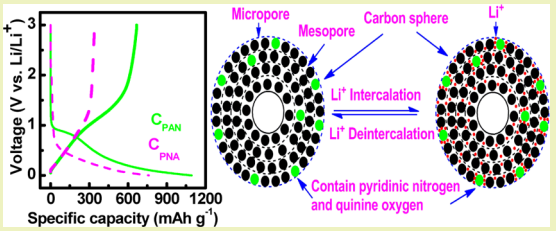

KEYWORDS: *Lignosulfonate, Polyaniline, Self-assembly, Low-cost, Anode, Lithium ion battery*

INTRODUCTION

Lignin, a waste from the bioethanol and pulping processing industries, has drawn lots of attention due to the energy crisis and environmental pollution. Yet, most are discharged or consumed directly as fuel, which results in serious environmental problems.[1] Therefore, it is meaningful to make full use of lignin not only for saving renewable natural resources but also for reducing pollution. Because of its abundance and low-cost, lignin has been applied in many fields, such as carbon materials,[2−6] adsorbents[7,8] and biofuel.[9] As carbon materials, however, lignin-based carbon materials have rarely been applied in anodes for lithium ion batteries. In fact, it is hard for these lignin-based carbon materials to exhibit high electrochemical performance because of their surface functional groups, structures, and morphologies.

Polyaniline (PANI) has been used as a precursor to prepare nitrogen-containing carbon materials[10−14] due to the advantages of PANI, such as low cost, unique chemical properties, and excellent thermal and environmental stability. For example, nitrogen-containing carbon nanotubes were easily prepared by the carbonization of PANI nanotubes,[15] and nitrogen-containing activated carbon prepared from PANIs has been used in supercapacitor electrodes.[10] Moreover, carbon nanowires,[11] carbon nanospheres,[12] carbon analogues,[13] and granular carbon[14] were also obtained from PANI by direct pyrolysis. The structure of nitrogen-containing carbon could be effortlessly changed by controlling the structure of PANI as a precursor. In addition, the attachment of bulky alkyl groups to PANI chains will lead to a decrease in the basicity of the amine nitrogen and will result in significant changes in both the geometric and electronic structure of PANI.[16]

In this work, nitrogen- and oxygen-containing carbon micro/nanospheres were prepared by direct pyrolysis of lignosulfonate/polyaniline (LS/PANI) and lignosulfonate/poly(*N*-ethylaniline) (LS/PNA) composite spheres. The use of lignosulfonate not only cuts down the cost of preparation of composite spheres but also reduces potential environment pollutions. Although the preparation of LS/PANI and LS/PNA composites and their carbon micro/nanospheres have been investigated in our previous works,[17,18] the effect of ethyl substituent on the electrochemical performances of nitrogen- and oxygen-containing carbon micro/nanospheres have not been investigated yet. These nitrogen- and oxygen-containing carbon micro/nanospheres are expected to exhibit different energy storage performances as anodes for lithium ion batteries.

Received: October 14, 2012
Revised: January 21, 2013
Published: January 31, 2013

EXPERIMENTAL SECTION

Materials. Aniline and *N*-ethylaniline (NA) monomers were purchased from Alfa Aesar and distilled under reduced pressure prior to use. Sodium lignosulfonate (LS), ammonium persulfate (APS), and other reagents were obtained from Sinopharm Chemical Reagent Co. Ltd. and used without further treatment.

Preparation of Composite Spheres. The LS/PANI and LS/PNA composite spheres were prepared by using an in situ polymerization from aniline[17] and *N*-ethylaniline,[18] respectively. The typical polymerization process for LS/PANI was as follows. Sodium lignosulfonate (0.93 g) was dissolved in HCl (1.0 M, 70 mL) aqueous solution in a glass flask. Then, aniline (0.91 mL) was added under stirring to form a mixture of aniline-LS. APS (2.28 g) was added separately in HCl (1.0 M, 30 mL) aqueous solution to prepare an oxidant solution. The APS solution was then poured into the above aniline−LS mixture solution at 25 °C, and the reaction was left at this temperature for 24 h. After the reaction, LS/PANI precipitate was thoroughly washed with an excess of deionized water several times to remove the residual oxidant and LS and water-soluble oligomeric products. A dark green product was left to dry in a vacuum at 60 °C for one week to obtain LS/PANI powder.

Preparation of Carbon Spheres. Carbonization of the LS/PANI and LS/PNA composite spheres was carried out under atmospheric pressure. The definite procedures were reported as follows: a corundum crucible containing a certain amount of the composite sample was put into a temperature-controlled furnace and then was heated to 700 °C with a heating rate of 3 °C min^{-1} under an argon flow and maintained at the desired temperature for 2 h, followed by cooling to 25 °C under an argon flow. Finally, the carbon spheres were obtained and labeled as C_{PAN} and C_{PNA}.

Characterization and Measurements. The bulk electrical conductivity of a pressed pellet with a thickness of 20−30 mm for the LS/PANI and LS/PNA composite sphere samples were measured at 25 °C using a four-probe technique. Fourier transform infrared spectroscopy (FTIR) spectra were recorded on a Nicolet FTIR 5700 spectrophotometer in KBr pellets. The carbon, hydrogen, and nitrogen weight percentages of samples were determined by using a Vario EL III elemental analyzer. Wide-angle X-ray diffraction (XRD) scans for C_{PAN} and C_{PNA} samples were obtained using an Ultima III X-ray model diffractometer (Rigaku, Japan) with Cu Kα radiation at a scanning rate of 10° min^{-1} in a reflection mode over a 2θ range from 5° to 70°. Morphological measurements were performed using scanning electron microscopy (SEM, Philips XL30 FEG), field emission scanning electron microscopy (FE-SEM, Carl Zeiss ULTRA 55 FESEM), and transmission electron microscopy (TEM, JEM-2010, Jeol). Pore structures of the samples were characterized by physical adsorption of N_2 at 77 K in a Micromeritics ASAP 2020 apparatus. Prior to analysis, the samples were outgassed at 120 °C for 12 h under vacuum to clean the surface. The surface area was obtained by the Brunauer−Emmett−Teller (BET) method. X-ray photoelectron spectroscopy (XPS) measurement was performed on a Thermo ESCALAB 250 high performance electron spectrometer using a monochromatic Al Kα as the excitation source.

Electrochemical Measurements. The electrochemical performances of the carbon spheres were evaluated in CR2025 coin cells. The test electrodes were made of active materials (85 wt %), acetylene black (10 wt %), and polyvinylidene fluoride (5 wt %). This mixture was coated on copper current collector. Lithium foil was served as a counter electrode. The separator was Cellgard 2320, and the electrolyte was 1 M $LiPF_6$ in a blended ethylene carbonate and dimethyl carbonate solution with volumetric ratio of 1:1. The batteries were charged and discharged in the potential range of 0.001−3.0 V vs Li/Li^+ at a constant current density of 60, 100, and 200 mA g^{-1} on the Land Battery Test System (Wuhan, China). All cells were assembled in a glovebox filled with highly pure argon gas and tested at room temperature.

RESULTS AND DISCUSSION

Morphology and Formation Mechanism of the Composites. The SEM images of LS/PANI and LS/PNA composite spheres are shown in Figure 1.

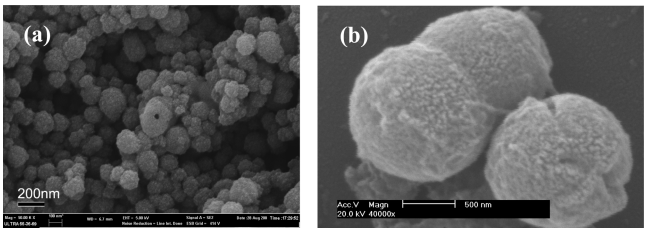

Figure 1. Figure 1. FESEM (a) and SEM (b) images of LS/PANI (a) and LS/PNA (b) composite spheres.

It was found that the average diameters of the LS/PANI and LS/PNA uniform spheres were about 180 and 1300 nm, respectively. The surfaces of these two spheres were rough and composed of a great many well-distributed nanoparticles. It indicated that these two uniform spheres might be formed via self-assembly of their nanoparticles. Moreover, there was an obvious small hole on the surface of the larger LS/PANI spheres (Figure 1a) that had been confirmed as hollow spheres.[19] Compared with the LS/PANI spheres, there were no holes found on the surface of the LS/PNA spheres (Figure 1b).

A possible formation mechanism of the two lignin-based uniform spheres is speculated in Scheme 1.

Scheme 1. Possible Formation Mechanism of the Two Lignin-Based Spheres

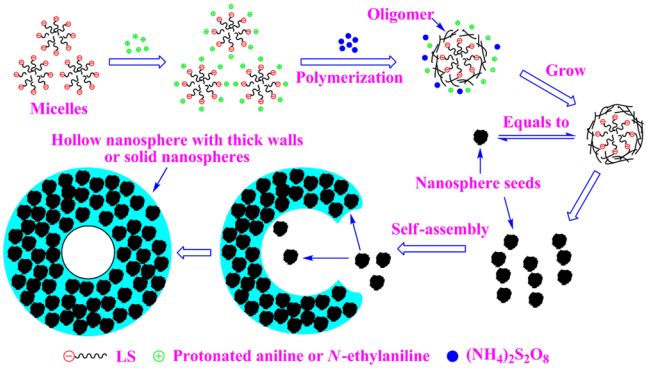

The detailed procedures were as follows. First, the negatively charged LS dissolved in the solution formed micelles, and protonated aniline was dispersed around micelles due to the ionic bonds. Then, when the ammonium persulfate was added, oligomers were obtained on the surface of micelles[20,21] and grew into nanosphere seeds. Last, these nanosphere seeds were self-assembled into hollow spheres with a hole. Of course, these hollow spheres might continue to grow into thick-shell hollow spheres or solid spheres via self-assembly with abundant nanosphere seeds.

It is also shown in Figure 1 that these two spheres had different diameters, which was due to the ethyl substituent effect on the structure of LS/PNA composite spheres. The bulk electrical conductivities of the LS/PANI and LS/PNA composite sphere samples were 2.63 and 0.12 S cm^{-1}, respectively. It could be found that the bulk electrical conductivity of the LS/PNA composite spheres was much

dx.doi.org/10.1021/sc300113w | ACS Sustainable Chem. Eng. 2013, 1, 334−340

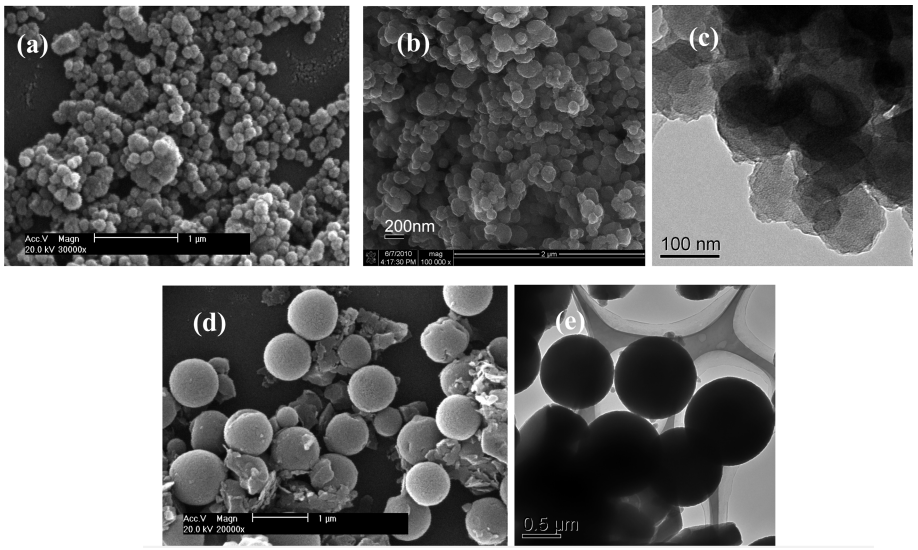

Figure 2. SEM (a,d), FESEM (b), and TEM (c,e) images of the C_{PAN} (a,b,c) and C_{PNA} (d,e) carbon spheres.

less than that of LS/PANI composite spheres. This was because the level of the nitrogen lone pair-π overlap between the ring orbitals and the lone pair decreased due to the ethyl substitution.[22] Compared with aniline, *N*-ethylaniline tends to form smaller nanosphere seeds than that of aniline owing to the steric hinerance and configuration of oligomers. Besides, *N*-ethylaniline monomers exhibit different polymerization rates compared with aniline monomers. Owing to the push electronic effect of *N*-ethyl, the nitrogen lone pair of *N*-ethylaniline monomer possessed more negative electrons than that of aniline monomer. As a result, the nitrogen lone pair with more negative electrons more easily reacted with the radical cations. Therefore, the *N*-ethylaniline monomer had higher reaction activity than aniline. Because of the different polymerization rates of aniline and *N*-ethylaniline, nanosphere seeds with different sizes could be found on the surface of the LS/PANI and LS/PNA composite spheres (Figure 1a,b). The nanosphere seed sizes of LS/PNA composite spheres were bigger than that of LS/PANI composite spheres, which was exactly in agreement with the reaction activity of monomers. Consequently, nanosphere seeds with different sizes were assembled into spheres with different sizes (Figure 1). In addition, the LS/PANI composite nanospheres with holes can be found in Figure 1a, whereas holes could hardly be found in the LS/PNA composite spheres (Figure 1b). Compared with LS/PANI composite nanospheres, LS/PNA composite spheres continued to assemble into solid spheres because of high reaction activity (Scheme 1). In short, the self-assembly process had much to do with the sizes of nanosphere seeds and the reaction activity of monomers.

Morphology and Structures of the Carbon Spheres. Figure 2 displays the SEM, FESEM, and TEM images of the C_{PAN} and C_{PNA} carbon spheres.

It is shown in Figure 2a,b that uniform C_{PAN} carbon nanospheres with the average diameter of 135 nm were obtained, while the surface of these carbon nanospheres was rough (Figure 2c). In addition, the average diameter of C_{PNA} carbon microspheres (700 nm) was much less than that of LS/PNA composite microspheres (1.3 μm), and some fragments of the C_{PNA} carbon microspheres were also observed (Figure 2d). These results showed the great shrinkage of LS/PNA composite microspheres and also indicated the destruction of LS/PNA spheres happened in the carbonization process.

FTIR spectra of the C_{PAN} and C_{PNA} carbon spheres were shown in Figure S1a of the Supporting Information. The peaks at about 3450 cm^{-1} might be assigned to adsorbed water because the −OH group and the presence of nitrogen in carbon spheres would increase the hydrophilicity.[13,14] The peaks at 1600 cm^{-1} were attributed to the stretching of quinoid.[19] However, the intensity of the peak at 1600 cm^{-1} of the C_{PAN} nanospheres was much stronger than that of the C_{PNA} carbon microspheres, which was possibly strengthened by weak oxygen containing functional groups (e.g., quinone groups). Moreover, peaks with slight intensity at 1036 cm^{-1} should be assigned to S═O symmetric stretching of the sulfonic group on the lignosulfonate chains, which would disappear with the carbonization temperature increasing.[18]

Wide-angle X-ray diffractograms of the C_{PAN} and C_{PNA} carbon spheres were investigated in Figure S1b of the Supporting Information. There were two broad diffraction peaks at around 25.4° and 43.5°, corresponding to (002) and (100) planes of micrographites, respectively.[23] The (002) planes of two carbon spheres show similar intensity of diffraction peaks. However, the intensity of the (100) plane was varied. The intensity of the (100) plane of the C_{PAN} nanospheres was higher than that of the C_{PNA} microspheres, which signified that the crystallite growth of the C_{PAN} nanospheres had a preferred orientation along the (100) plane comparing to the C_{PNA} microspheres. In addition, the (002) plane of the C_{PNA} microspheres had a trend moving toward a bigger bragg angle. The distance between the (002) planes, d_{002}, was calculated using the Bragg equation ($\lambda = 2d_{002}\sin\theta_{002}$). The d_{002} of the C_{PAN} and C_{PNA} carbon spheres was 0.356 and 0.337 nm, respectively. These results revealed that the crystallite growth of the C_{PNA} carbon microspheres was much more than that of the C_{PAN} carbon nanospheres in the carbonization process. This indicated the access for Li^+ ions intercalation and deintercalation of the C_{PAN} carbon nanospheres was much bigger than that of C_{PNA} carbon microspheres, which also signified that the electrochemical performance of C_{PAN} carbon nanospheres might be better than that of C_{PNA} carbon microspheres.

Table 1 lists the elemental analysis data of the C_{PAN} and C_{PNA} carbon spheres. It could be found that the content of carbon element of C_{PAN} and C_{PNA} was of 81.59% and 73.07%, respectively, while that in monomer was 77.42% and 79.34%, respectively. This indicated that the C_{PAN} nanospheres probably had more stable structures and thermal properties, whereas the content of carbon element of the C_{PNA} microspheres had a minor reduction.

Table 1. Elemental Analysis Data of C_{PAN} and C_{PNA} Carbon Spheres

	element mass (%)		
samples	carbon	nitrogen	hydrogen
C_{PAN}	81.59	8.78	1.90
C_{PNA}	73.07	7.60	1.38

In addition, the content of the nitrogen element of the C_{PAN} and C_{PNA} carbon spheres was of 8.78% and 7.60%, respectively, which was lower than the original nitrogen content in their monomers. The loss of nitrogen content of the carbon spheres was due to the release of nitrogen-containing small molecules and remaining nitrogen formed as the functional groups on the surface of carbon spheres. Therefore, it could be speculated that the C_{PAN} carbon nanospheres with the higher content of nitrogen might possess better performance as the anode of lithium ion batteries.[15]

Surface areas of the C_{PAN} and C_{PNA} carbon spheres were 291.6 and 37.86 $m^2\ g^{-1}$, respectively, which were investigated using the Bruauer–Emmett–Teller (BET) equation. It was found that the surface areas depended on the surface roughness and diameters of the carbon spheres (Table 2).

Table 2. Characteristics of Pore Structures of the C_{PAN} and C_{PNA} Carbon Spheres

samples	S_{BET}[a] ($m^2\ g^{-1}$)	D_a[b] (nm)	V_{micro}[c] ($cm^3\ g^{-1}$)	V_{meso}[d] ($cm^3\ g^{-1}$)	Vt[e] ($cm^3\ g^{-1}$)
C_{PAN}	291.6	4.48	0.13	0.19	0.32
C_{PNA}	37.86	2.79	0.0085	0.0175	0.026

[a]Specific surface area determined according to the BET equation. [b]Adsorption average pore diameter (4 V/A by BET). [c]Volume of micropores. [d]Volume of mesopores. [e]Total pore volume.

According to the morphologies of the C_{PAN} and C_{PNA} carbon spheres in Figure 2, the carbon spheres with rougher surfaces and smaller diameters had bigger surface areas. The total pore volume was estimated from the amount adsorbed at a relative pressure of 0.98. The average pore diameters of the C_{PAN} and C_{PNA} carbon spheres were 4.48 and 2.79 nm, respectively. However, the micropores and mesopores of the C_{PNA} microspheres were significantly less than that of the C_{PAN} carbon nanospheres. On the one hand, this was due to the fewer surface areas of the C_{PNA} carbon microspheres. On the other hand, the LS/PNA composite spheres would shrink gradually in the carbonization process, and some micropores and mesopores might disappear with the carbonization temperature increasing.

The XPS spectra of the C_{PAN} and C_{PNA} carbon spheres were demonstrated in Figure 3. The C1s spectrum of the C_{PAN} carbon nanospheres had three distinct component peaks at binding energy of 284.7, 286.3, and 288 eV, corresponding to graphitic carbon, C–O and C–OH groups, and the carbonyl group, respectively.[24] However, the C1s spectra of the C_{PNA} carbon microspheres were lacking the peak at binding energy of 288 eV, indicating that there were few C=O group in the C_{PNA} carbon microspheres. This was most possibly because the places for the formation of quinone oxygen were held or prevented by the ethyl substituent in the *N*-position of poly(*N*-ethylaniline). The O1s spectra of the C_{PAN} and C_{PNA} carbon spheres had the same peak at the binding of 532.3 eV, which was assigned to hydroxyl (C–OH) and ether (C–O–C) groups.[25] In addition, the O1s spectrum of the C_{PAN} carbon nanospheres showed a peak at the binding energy of 531.1 eV, representing carbonyl and/or quinone groups (O–I) corresponding to the C1s spectrum of the C_{PAN} carbon nanospheres, whereas the O1s spectra of the C_{PNA} carbon microspheres had the peak at the binding of 534 eV, representing chemisorbed oxygen and/or water (O–IV).[26]

As for N1s spectra, there were two equal peaks of the C_{PAN} and C_{PNA} carbon spheres, including N-6 (pyridinic nitrogen, 398.7 ± 0.3 eV) and N-Q (quaternary nitrogen, 401.4 ± 0.5 eV).[27] The pyridinic nitrogen along with quinone oxygen were reported as the most important functional groups affecting energy storage performance.[28] However, there was only the C_{PAN} carbon nanospheres possessing both such functional groups, implying the C_{PAN} carbon nanospheres as the anodes

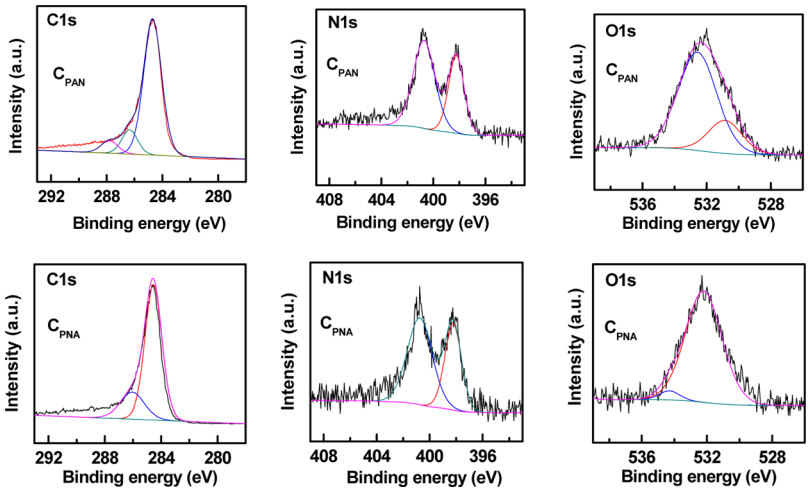

Figure 3. X-ray photoelectron spectra of the C_{PAN} and C_{PNA} carbon spheres.

dx.doi.org/10.1021/sc300113w | ACS Sustainable Chem. Eng. 2013, 1, 334–340

for lithium ion batteries would have better performance than that of the C_{PNA} carbon microspheres.

Electrochemical Performances. The charge/discharge characteristics of the first cycle of the C_{PAN} and C_{PNA} carbon spheres at a current density of 100 mA g^{-1} are illustrated in Figure 4a.

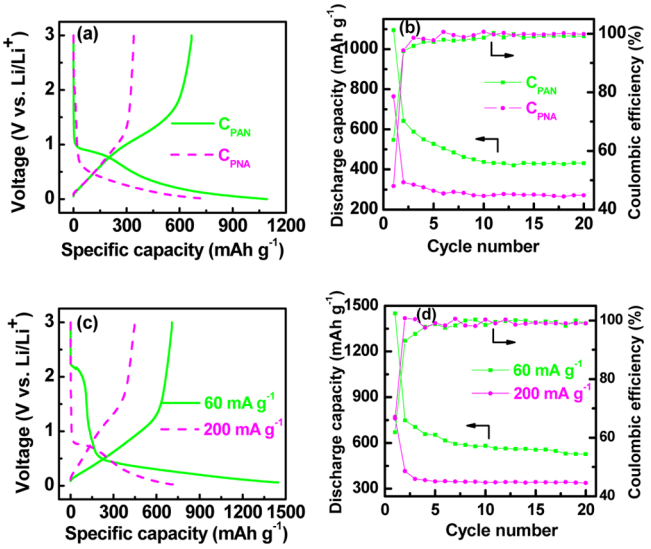

Figure 4. First cycle of charge/discharge profiles (a) and cycling performances (b) of the C_{PAN} and C_{PNA} carbon spheres at a constant current density of 100 mA g^{-1}. First cycle of charge/discharge profiles (c) and cycling performances (d) of the C_{PAN} carbon spheres at a constant current density of 60 and 200 mA g^{-1}.

The first charge/discharge cycle curves of the C_{PAN} and C_{PNA} carbon spheres exhibited a discharge capacity of 1094 and 846 mAh g^{-1}, respectively, and a charge capacity of 698 and 434 mAh g^{-1}, respectively. The discharge capacity and Coulombic efficiency of these carbon spheres at a current density of 100 mA g^{-1} in 20 cycles are displayed in Figure 4b. The first Coulombic efficiency of the two samples was of 63.8% and 51.3%, respectively. From the second cycle, however, the Coulombic efficiency went up to 94.1% and 94.3%, respectively. With the cycling, the Coulombic efficiency almost reached 100%. After 20 cycles, the discharge capacity of the C_{PAN} and C_{PNA} carbon spheres was 431 and 271 mAh g^{-1}, respectively. This indicated that the ethyl substituent had a profound effect on the structures of the C_{PNA} carbon microspheres and furthermore affected their discharge capacity after 20 cycles.

In order to investigate various charge/discharge rates of the C_{PAN} carbon nanospheres, the first cycle at a current density of 60 and 200 mA g^{-1} are illustrated in Figure 4c, respectively. Compared with a current density of 100 mA g^{-1}, the first charge/discharge cycle curves of the C_{PAN} carbon spheres at a current density of 60 and 200 mA g^{-1} exhibited a discharge capacity of 1450 and 770 mAh g^{-1}, respectively, and a charge capacity of 707 and 446 mAh g^{-1}, respectively. The discharge capacity and Coulombic efficiency of the C_{PAN} carbon spheres at a current density of 60 and 200 mA g^{-1} in 20 cycles are displayed in Figure 4d. The first Coulombic efficiency of the C_{PAN} carbon spheres at a current density of 60 and 200 mA g^{-1} was of 61.9% and 66.6%, respectively. From the second cycle, however, the Coulombic efficiency went up to 93.1% and 100%, respectively. After 20 cycles, the discharge capacity of the C_{PAN} carbon spheres at a current density of 60 and 200 mA g^{-1} was 526 and 338 mAh g^{-1}, respectively. This indicated that charge/discharge rates would significantly influence the charge/discharge capacity of the C_{PAN} carbon spheres.

A possible mechanism of Li^+ intercalation and deintercalation in the two carbon spheres with different amounts of micropores and mesopores is discussed in Scheme 2. The procedure was as follows. First, Li^+ ions intercalated into the micropores through mesopores, for the micropores in the carbon spheres might act as reservoirs for lithium storage, while the mesopores provided an access to the transportation and diffusion of lithium ions.[15] Second, the most important functional groups, such as pyridinic nitrogen and quinone oxygen, played important roles in improving the specific capacity of anode materials.[28]

The specific capacity of the C_{PAN} and C_{PNA} carbon spheres as anodes for lithium ion batteries depended on two main factors: the structure of carbon spheres and surface functional groups. The differences between the structures of the two types of carbon spheres had much to do with that of their composite spheres, which was due to the ethyl substituent effect.[18] Moreover, an ethyl substituent in the *N*-position of LS/PNA composite spheres would hinder the acid/base reaction.[29]

Therefore, the intercalation/deintercalation of the lithium ions in the C_{PNA} carbon microspheres could be affected. Between the two types carbon spheres, the C_{PAN} nanospheres with larger surface areas possessed better electrochemical performance, for a large surface area was beneficial to improve capacity.[30] Furthermore, the C_{PAN} carbon nanospheres had different types of C1s and O1s comparing with the C_{PNA} carbon microspheres according to the XPS analysis. It revealed that the C_{PAN} nanospheres contained more pyridinic nitrogen and quinone oxygen functional groups, which was beneficial to improve their electrochemical performance. In conclusion, the C_{PAN} carbon nanospheres had a better electrochemical performance as anodes for lithium ion batteries than did C_{PNA} carbon microspheres.

CONCLUSIONS

Nitrogen- and oxygen-containing C_{PAN} and C_{PNA} carbon micro/nanospheres were obtained by pyrolysis from two lignin-based composite spheres at temperature of 700 °C. The ethyl substituent had a significant effect on the structures of LS/PNA composite and their carbon spheres because of the steric and electronic effects of the alkyl substituents. The C_{PAN}

Scheme 2. Possible Mechanism of Li^+ Intercalation and Deintercalation for the C_{PAN} and C_{PNA} Carbon Spheres

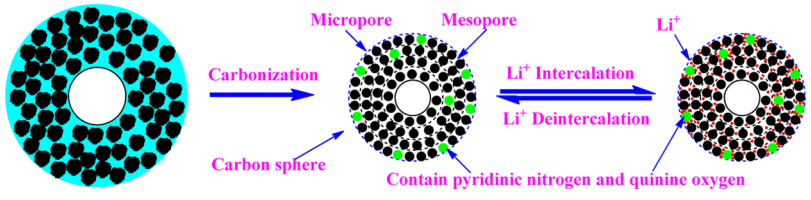

dx.doi.org/10.1021/sc300113w | ACS Sustainable Chem. Eng. 2013, 1, 334−340

nanospheres possessed higher surface areas, more micropores and mesopores, and more nitrogen- and oxygen-containing functional groups. Therefore, the C_{PAN} carbon nanospheres displayed better electrochemical performance in lithium ion batteries than the C_{PNA} carbon microspheres. The first charge capacity and discharge capacity of the C_{PAN} nanospheres at a current density of 60, 100, and 200 mA g^{-1} exhibited a discharge capacity of 1450, 1094, and 770 mAh g^{-1}, respectively, and a charge capacity of 707, 698, and 446 mAh g^{-1}, respectively. Furthermore, they still owned a high discharge capacity at a current density of 60, 100, and 200 mA g^{-1} of 526, 431, and 338 mAh g^{-1}, respectively, after 20 cycles, having a trend to keep constant specific capacitance. These results showed the low-cost C_{PAN} carbon nanospheres prepared from lignin-based composite spheres have a potential application as an anode material for high performance lithium ion batteries.

■ ASSOCIATED CONTENT

Supporting Information

FTIR spectra and X-ray diffractograms of the C_{PAN} and C_{PNA} carbon spheres. This material is available free of charge via the Internet at http://pubs.acs.org.

■ AUTHOR INFORMATION

Corresponding Author

*E-mail: qiufenglv@163.com; qiufenglvfzu@gmail.com.

Notes

The authors declare no competing financial interest.

■ ACKNOWLEDGMENTS

This work was supported by the National Natural Science Foundation of China (51272045), Natural Science Foundation of Fujian Province, China (2012J01201), and Science-Technology Foundation of Education Bureau of Fujian Province, China (JA12031).

■ REFERENCES

(1) Wu, Y.; Zhang, S.; Guo, X.; Huang, H. Adsorption of chromium(III) on lignin. *Bioresour. Technol.* **2008**, *99*, 7709−7715.

(2) Kadla, J. F.; Kubo, S.; Venditti, R. A.; Gilbert, R. D.; Compere, A. L.; Griffith, W. Lignin-based carbon fibers for composite fiber applications. *Carbon* **2002**, *40*, 2913−2920.

(3) Kubo, S.; Kadla, J. F. Lignin-based carbon fibers: Effect of synthetic polymer blending on fiber properties. *J. Polym. Environ.* **2005**, *13*, 97−105.

(4) Babeł, K.; Jurewicz, K. KOH activated lignin based nanostructured carbon exhibiting high hydrogen electrosorption. *Carbon* **2008**, *46*, 1948−1956.

(5) Kijima, M.; Hirukawa, T.; Hanawa, F.; Hata, T. Thermal conversion of alkaline lignin and its structured derivatives to porous carbonized materials. *Bioresour. Technol.* **2011**, *102*, 6279−6295.

(6) Mussatto, S. I.; Fernandes, M.; Rocha, G. J. M.; Órfão, J. J. M.; Teixeira, J. A.; Roberto, I. C. Production, characterization and application of activated carbon from brewer's spent grain lignin. *Bioresour. Technol.* **2010**, *101*, 2450−2457.

(7) Suhas; Carrott, P. J. M.; Ribeiro Carrott, M. M. L. Lignin − from natural adsorbent to activated carbon: A review. *Bioresour. Technol.* **2007**, *98*, 2301−2312.

(8) He, Z.-W.; Lü, Q.-F.; Zhang, J.-Y. Facile preparation of hierarchical polyaniline-lignin composite with a reactive silver-ion adsorbability. *ACS Appl. Mater. Interfaces* **2012**, *4*, 369−374.

(9) Gellerstedt, G. r.; Li, J.; Eide, I.; Kleinert, M.; Barth, T. Chemical structures present in biofuel obtained from lignin. *Energy Fuels* **2008**, *22*, 4240−4244.

(10) Li, L.; Liu, E.; Li, J.; Yang, Y.; Shen, H.; Huang, Z.; Xiang, X.; Li, W. A doped activated carbon prepared from polyaniline for high performance supercapacitors. *J. Power Sources* **2010**, *195*, 1516−1521.

(11) Yuan, D.-s.; Zhou, T.-x.; Zhou, S.-l.; Zou, W.-j.; Mo, S.-s.; Xia, N.-n. Nitrogen-enriched carbon nanowires from the direct carbonization of polyaniline nanowires and its electrochemical properties. *Electrochem. Commun.* **2011**, *13*, 242−246.

(12) Han, C.-C.; Bai, M.-Y.; Yang, K.-F.; Lee, Y.-S.; Lin, C.-W. A novel method for making highly dispersible conducting polymer and concentric graphitic carbon nano-spheres based on an undoped and functionalized polyaniline. *J. Mater. Chem.* **2008**, *18*, 3918−3925.

(13) Stejskal, J.; Trchová, M.; Hromádková, J.; Kovářová, J.; Kalendová, A. The carbonization of colloidal polyaniline nanoparticles to nitrogen-containing carbon analogues. *Polym. Int.* **2010**, *59*, 875−878.

(14) Rozlívková, Z.; Trchová, M.; Exnerová, M.; Stejskal, J. The carbonization of granular polyaniline to produce nitrogen-containing carbon. *Synth. Met.* **2011**, *161*, 1122−1129.

(15) Xiang, X.; Huang, Z.; Liu, E.; Shen, H.; Tian, Y.; Xie, H.; Wu, Y.; Wu, Z. Lithium storage performance of carbon nanotubes prepared from polyaniline for lithium-ion batteries. *Electrochim. Acta* **2011**, *56*, 9350−9356.

(16) Wei, Y.; Focke, W. W.; Wnek, G. E.; Ray, A.; MacDiarmid, A. G. Synthesis and electrochemistry of alkyl ring-substituted polyanilines. *J. Phys. Chem.* **1989**, *93*, 495−499.

(17) Lü, Q.-F.; He, Z.-W.; Zhang, J.-Y.; Lin, Q. Preparation and properties of nitrogen-containing hollow carbon nanospheres by pyrolysis of polyaniline−lignosulfonate composites. *J. Anal. Appl. Pyrolysis* **2011**, *92*, 152−157.

(18) He, Z.-W.; Lü, Q.-F.; Lin, Q. Fabrication of poly(*N*-ethylaniline)/lignosulfonate composites and their carbon microspheres. *Int. J. Biol. Macromol.* **2012**, *51*, 946−952.

(19) Lü, Q.; Wang, C.; Cheng, X. One-step preparation of conductive polyaniline-lignosulfonate composite hollow nanospheres. *Microchim. Acta* **2010**, *169*, 233−239.

(20) Stejskal, J.; Sapurina, I.; Trchová, M. Polyaniline nanostructures and the role of aniline oligomers in their formation. *Prog. Polym. Sci.* **2010**, *35*, 1420−1481.

(21) Stejskal, J.; Sapurina, I.; Trchová, M.; Konyushenko, E. N. Oxidation of aniline: polyaniline granules, nanotubes, and oligoaniline microspheres. *Macromolecules* **2008**, *41*, 3530−3536.

(22) Zaidi, N. A.; Foreman, J. P.; Tzamalis, G.; Monkman, S. C.; Monkman, A. P. Alkyl substituent effects on the conductivity of polyaniline. *Adv. Funct. Mater.* **2004**, *14*, 479−486.

(23) Lin, Q.; Tang, H.; Guo, D.; Zheng, M. Preparation and properties of carbon microbeads by pyrolysis of *N*-phenyl maleimide modified novolac resin. *J. Anal. Appl. Pyrolysis* **2010**, *87*, 276−281.

(24) Gu, L.; Zhang, X.; Lei, L. Degradation of aqueous p-nitrophenol by ozonation integrated with activated carbon. *Ind. Eng. Chem. Res.* **2008**, *47*, 6809−6815.

(25) Seredych, M.; Hulicova-Jurcakova, D.; Lu, G. Q.; Bandosz, T. J. Surface functional groups of carbons and the effects of their chemical character, density and accessibility to ions on electrochemical performance. *Carbon* **2008**, *46*, 1475−1488.

(26) Xiang, X.; Liu, E.; Li, L.; Yang, Y.; Shen, H.; Huang, Z.; Tian, Y. Activated carbon prepared from polyaniline base by K_2CO_3 activation for application in supercapacitor electrodes. *J. Solid State Electrochem.* **2011**, *15*, 579−585.

(27) Nowicki, P.; Pietrzak, R.; Wachowska, H. X-ray photoelectron spectroscopy study of nitrogen-enriched active carbons obtained by ammoxidation and chemical activation of brown and bituminous coals. *Energy Fuels* **2009**, *24*, 1197−1206.

(28) Hulicova-Jurcakova, D.; Seredych, M.; Lu, G. Q.; Bandosz, T. J. Combined effect of nitrogen- and oxygen-containing functional groups of microporous activated carbon on its electrochemical performance in supercapacitors. *Adv. Funct. Mater.* **2009**, *19*, 438−447.

(29) Yağan, A.; Pekmez, N. Ö.; Yıldız, A. Electropolymerization of poly(*N*-ethyl aniline) on mild steel: Synthesis, characterization and corrosion protection. *Electrochim. Acta* **2006**, *51*, 2949−2955.

(30) Kim, C.; Yang, K. S.; Kojima, M.; Yoshida, K.; Kim, Y. J.; Kim, Y. A.; Endo, M. Fabrication of electrospinning-derived carbon nanofiber webs for the anode material of lithium-ion secondary batteries. *Adv. Funct. Mater.* **2006**, *16*, 2393−2397.